with the Shanks' transformation. It is known that it works effectively for slowly convergent series with sign-alternating terms [13]. However, the Kummer's method of the 2nd order provides rather fast convergence, and, therefore, additional application of the Shanks' transformation, that itself requires performing additional operations, would only complicate the algorithm and give weak effect. If we neglect that effect and suppose that the computation times for the Kummer's method of the 2nd order in [9] and here are identical at the point $x = y = 0$, then the curves corresponding to the Ewald's method taken from [9] will occupy the positions as shown in Figs. 3 and 4. The supposition made above does not allow drawing an unambiguous conclusion here on the effectiveness of the Kummer's method of the 2nd order with respect to the Ewald method. That point still require a more careful additional study. However we can conclude now that the Kummer's method of the 4th order already explicitly excels the Ewald method for the indicated values of the relative error. For this reason, we did not carry out calculations with using the Kummer's method of the 6th order providing even higher effectiveness. The values of the maximum relative error considered here are already quite acceptable for practical calculations of the Green's function. With decreasing the specified values for the error, the Ewald method, providing Gaussian convergence rate, can turn out to be more effective than the 4th order Kummer's method. In that case, it would be appropriate to compare it with the Kummer's method of the 6th order.

ACKNOWLEDGMENT

The authors are grateful to Dr. A. Galli and his colleagues of "La Sapienza" University of Rome, Italy, for exchange of the views regarding determination of the relative error.

REFERENCES

[1] N. Amitay, V. Galindo, and C.-P. Wu, *Theory and Analysis of Phased Array Antennas*. New York: Wiley, 1972.

[2] , T. K. Wu, Ed., *Frequency Elective Surface and Grid Array*. New York: Wiley, 1995.

[3] C.-F. Yang, W. D. Burnside, and R. C. Rudduck, "A doubly periodic moment method solution for the analysis and design of an absorber covered wall," *IEEE Trans. Antennas Propag.*, vol. 41, no. 5, pp. 600–609, May 1993.

[4] G. Valerio, P. Baccarelli, P. Burghignoli, and A. Galli, "Comparative analysis of acceleration techniques for 2-D and 3-D Green's functions in periodic structures along one and two directions," *IEEE Trans. Antennas Propag.*, vol. 55, no. 6, pt. 1, pp. 1630–1643, Jun. 2007.

[5] S. P. Skobelev, "Comments on Comparative analysis of acceleration techniques for 2-D and 3-D Green's functions in periodic structures along one and two directions," *IEEE Trans. Antennas Propag.*, vol. 55, no. 12, p. 3746, Dec. 2007.

[6] M. M. Ivanishin, "Use of integral equations in the problem on a cylinder inside a rectangular waveguide," *Radio Eng. Electr. Phys.*, vol. 29, no. 12, pp. 1–8, 1984.

[7] S. P. Skobelev and L. L. Mukhamedov, "Analysis of waveguide antenna arrays with protruding dielectric elements," *IEEE Trans. Antennas Propag.*, vol. 41, no. 5, pp. 574–581, May 1993.

[8] S. P. Skobelev, "Performance of Yagi-Uda elements in planar array antennas for limited-scan applications," *Microw. Opt. Technol. Lett.*, vol. 34, no. 2, pp. 141–145, Jul. 2002.

[9] G. Valerio, P. Baccarelli, P. Burghignoli, and A. Galli, "Reply to 'Comments on Comparative analysis of acceleration techniques for 2-D and 3-D Green's functions in periodic structures along one and two directions," *IEEE Trans. Antennas Propag.*, vol. 55, no. 12, p. 3747, Dec. 2007.

[10] P. P. Ewald, "Die berechnung optischer und elektrostatischer gitterpotentiale," *Ann. Phys.*, vol. 64, pp. 253–287, 1921.

[11] M. M. Ivanishin, Personal Communication, Dec. 24, 2007.

[12] R. E. Jorgenson and R. Mittra, "Efficient calculation of the free space periodic Green's function," *IEEE Trans. Antennas Propag.*, vol. 38, no. 5, pp. 633–642, May 1990.

[13] S. Singh, W. F. Richards, J. R. Zinecker, and D. R. Wilton, "Accelerating the convergence of series representing the free space periodic Green's function," *IEEE Trans. Antennas Propag.*, vol. 38, no. 12, pp. 1958–1962, Dec. 1990.

[14] W. F. Richards, "The Green's function for an infinite periodic array of transverse dyadic dipoles in free space," *Personal Notes*, Jul. 1982.

[15] J. R. Zinecker, "Efficient computation of Green's functions for periodic structures," Master's thesis, Dept. Elec. Eng., Univ., Houston, TX, 1985.

[16] F. Capolino, D. R. Wilton, and W. A. Johnson, "Efficient computation of the 2-D Green's function for 1-D periodic structures using the ewald method," *IEEE Trans. Antennas Propag.*, vol. 53, no. 9, pp. 2977–2984, Sep. 2005.

Continuously Inhomogeneous Higher Order Finite Elements for 3-D Electromagnetic Analysis

Milan M. Ilić, Andjelija Ž. Ilić, and Branislav M. Notaroš

***Abstract*—A novel higher order entire-domain finite element technique is presented for accurate and efficient full-wave three-dimensional (3-D) analysis of electromagnetic structures with continuously inhomogeneous material regions, using large generalized curved hierarchical curl-conforming hexahedral vector finite elements that allow continuous change of medium parameters throughout their volumes. This is the first general 3-D implementation and numerical demonstration of the inherent theoretical ability of the finite element method (FEM) to directly treat arbitrarily (continuously) inhomogeneous materials. The results demonstrate considerable reductions in both number of unknowns and computation time of the entire-domain FEM modeling of continuously inhomogeneous materials over piecewise homogeneous models. They indicate that, in addition to theoretical relevance and interest, large curved higher order continuous-FEM elements also have great potential for practical applications that include structures with pronounced material inhomogeneities and complexities.**

***Index Terms*—Computer-aided analysis, electromagnetic analysis, electromagnetic scattering, finite element method, higher order elements, inhomogeneous media, method of moments.**

I. INTRODUCTION

The finite element method (FEM) [1]–[3] in its various forms and implementations has been effectively used in full-wave three-dimensional (3-D) computations based on discretizing partial differential equations in electromagnetics for about four decades. FEM methodologies and

Manuscript received September 26, 2008; revised February 20, 2009. First published July 10, 2009; current version published September 02, 2009. This work was supported in part by the National Science Foundation under Grants ECCS-0647380 and ECCS-0650719, and in part by the Serbian Ministry of Science and Technological Development under Grant ET-11021.

M. M. Ilić is with the School of Electrical Engineering, University of Belgrade, 11120 Belgrade, Serbia and also with the Department of Electrical and Computer Engineering, Colorado State University, Fort Collins, CO 80523-1373 USA (e-mail: milanilic@etf.rs).

A. Ž. Ilić is with the Laboratory of Physics 010, Vinča Institute of Nuclear Sciences, 11001 Belgrade, Serbia (e-mail: andjelijailic@ieee.org).

B. M. Notaroš is with the Department of Electrical and Computer Engineering, Colorado State University, Fort Collins, CO 80523-1373, USA (fax: 970-491-2249, e-mail: notaros@colostate.edu).

Color versions of one or more of the figures in this paper are available online at http://ieeexplore.ieee.org.

Digital Object Identifier 10.1109/TAP.2009.2027350

0018-926X/$26.00 © 2009 IEEE

Authorized licensed use limited to: Branislav Notaros. Downloaded on September 2, 2009 at 04:23 from IEEE Xplore. Restrictions apply.

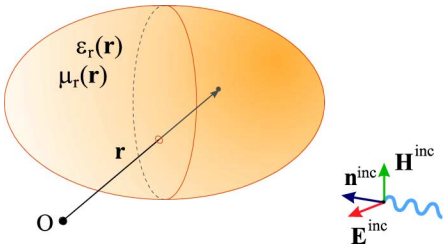

Fig. 1. Electromagnetic structure with continuously inhomogeneous materials in the FEM computational domain.

techniques are especially efficient in modeling and analysis of structures that contain inhomogeneous and complex electromagnetic materials, and the FEM is well established as a method of choice for such applications. Practically every FEM technique, within a really abundant and impressive body of work in the field, derives the theory and develops the FEM equations taking the advantage of the inherent ability of the FEM to directly treat continuously inhomogeneous materials. This property would allow that the material parameters, complex permittivity and permeability, of an electromagnetic structure can be arbitrary functions of spatial coordinates in the FEM computational domain, e.g., $\varepsilon(\mathbf{r})$ and $\mu(\mathbf{r})$, with $\mathbf{r}$ standing for the position vector of a point in the adopted coordinate system, as illustrated in Fig. 1. However, it appears that there is not a single 3-D FEM technique or code that actually implements $\varepsilon(\mathbf{r})$ and $\mu(\mathbf{r})$ as such, and enables direct computation on 3-D vector finite elements that include arbitrarily (continuously) inhomogeneous materials. Also, there seems to be no reported results of direct FEM analysis of continuously inhomogeneous 3-D closed- or open-region problems. Instead, FEM computations are carried out on piecewise homogeneous approximate models of the inhomogeneous structures, with $\varepsilon(\mathbf{r})$ and $\mu(\mathbf{r})$ replaced by appropriate piecewise constant approximations. Notable exceptions are a continuously inhomogeneous model with 2-D curvilinear scalar elements for magnetostatic analysis [4] and 1-D continuously inhomogeneous elements for uniform plane wave propagation problems [5]–[7].

In addition to considerable theoretical importance and interest, numerical modeling employing continuously inhomogeneous finite elements may find practical application in analysis of a broad range of devices, systems, and phenomena in electromagnetics. In antennas and propagation, the applications include antennas with continuously inhomogeneous substrates [8], scattering and diffraction from inhomogeneous dielectric lenses used in lens antennas (e.g., Luneburg and Maxwell lenses whose design is ultimately based on continuously changing permittivity profiles [9]), propagation in the ionosphere [10] and inhomogeneous plasmas [11], and absorbing coatings for reduction of radar cross sections of targets. In electronics and optics, examples may be processes in semiconductors with variety of doping profiles used for fabrication of solid-state microelectronic devices, optical integrated circuits that include devices with continuously changing refractive indices, such as inhomogeneous diffused optical waveguides [12], and radially inhomogeneous optical fibers [13]. Another group of applications includes inverse scattering problems, non-destructive testing applications, microwave imaging, and electromagnetic interaction with continuously changing biological tissues and materials (e.g., tomography [14]). In addition, with increasing interest in electromagnetic metamaterials, FEM techniques for efficient simulation of structures with arbitrary permittivity and permeability profiles could effectively be applied in designs and engineering of new artificial materials with desired properties beyond "standard" or natural media. Finally, purely mathematical materials widely used as artificial absorbers or perfectly matched layers (PMLs) for finite difference or finite element mesh truncation may also be added to the class of continuously inhomogeneous electromagnetic media, as they typically have linearly or quadratically (or otherwise optimized) changing parameters [15], [16].

From the numerical discretization point of view, modeling flexibility of continuously inhomogeneous finite elements can be fully exploited only if they can be made electrically large, which implies the use of higher order field expansions within the elements. Namely, if a low-order FEM technique is used, the elements must be electrically very small (on the order of a tenth of the wavelength in each dimension), because the fields are approximated by low-order basis functions. Subdivision of the structure using such elements results in a discretization of the permittivity and permeability profiles as well, so elements can be treated as homogeneous (i.e., their treatment as inhomogeneous would practically have no effect on the results). On the other side, higher order FEM techniques [17]–[25] (note that a much more comprehensive list of techniques is provided in [26]) enable p -refinement of the solution. This, in general, may greatly reduce the number of unknowns and enhance the accuracy and efficiency of the analysis, and, in particular, lets us use large geometrical elements (e.g., on the order of a wavelength in each dimension), so that a possible development and implementation of large continuously inhomogeneous finite elements seem to be both straightforward and efficient. We refer to the direct FEM computation on such elements as the entire-domain or large-domain analysis.

This paper presents a novel higher order entire-domain FEM technique for efficient 3-D analysis in the frequency domain of electromagnetic structures with continuously inhomogeneous material regions, based on Lagrange-type generalized curved parametric hexahedral elements of arbitrary geometrical orders for the approximation of geometry in conjunction with higher order curl-conforming hierarchical polynomial vector basis functions of arbitrary orders for the approximation of fields within the elements. Variations of medium parameters are incorporated by means of the same Lagrange interpolating scheme used for defining element spatial coordinates. The technique enables using as large as about two wavelengths on a side curved FEM hexahedra with arbitrary material inhomogeneities as building blocks for modeling of the structure. It represents an extension of our higher order FEM method in [20], and, to the best of our knowledge, this is the first direct 3-D FEM analysis of continuously inhomogeneous materials. In analysis of open-region problems, the FEM domain is truncated by hybridization with the method of moments (MoM) [27], [28]. Although the primary goal of this work is to numerically demonstrate that the FEM can indeed directly treat arbitrarily inhomogeneous regions, accurately, and as the first 3-D implementation of continuous-FEM modeling and analysis in high-frequency applications, the results in fact indicate that large curved higher order continuous-FEM elements, being computationally efficient, also have great potential for practical applications that include structures with pronounced material inhomogeneities and complexities.

II. Numerical Method

In our analysis method, the computational domain in Fig. 1 is first tessellated using geometrical elements in the form of Lagrange-type generalized curved parametric hexahedra of arbitrary geometrical orders K_u, K_v, and $K_w (K_u, K_v, K_w \geq 1)$, analytically described as [20]

$$\mathbf{r}(u,v,w) = \sum_{i=0}^{K_u}\sum_{j=0}^{K_v}\sum_{k=0}^{K_w} \mathbf{r}_{ijk} L_i^{K_u}(u) L_j^{K_v}(v) L_k^{K_w}(w)$$

$$L_i^{K_u}(u) = \prod_{\substack{l=0 \\ l\neq i}}^{K_u} \frac{u-u_l}{u_i-u_l}, \quad -1 \leq u,v,w \leq 1 \tag{1}$$

where $\mathbf{r}_{ijk} = \mathbf{r}(u_i, v_j, w_k)$ are position vectors of interpolation nodes and $L_i^{K_u}$ represent Lagrange interpolation polynomials in the u coor-

Authorized licensed use limited to: Branislav Notaros. Downloaded on September 2, 2009 at 04:23 from IEEE Xplore. Restrictions apply.

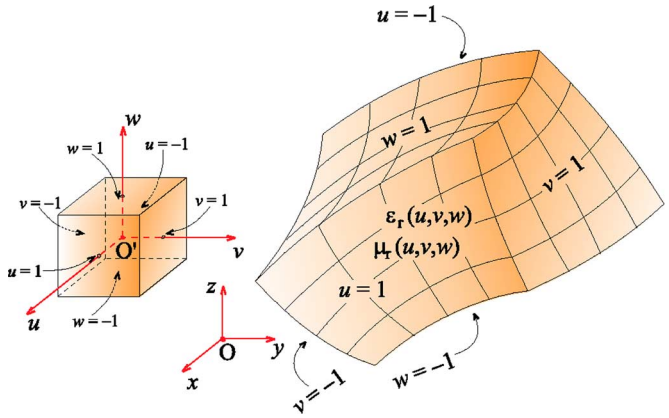

Fig. 2. Generalized curved parametric hexahedron defined by (1), with continuous variations of medium parameters given by (2); Cubical parent domain is also shown.

dinate, with u_l being the uniformly spaced interpolating nodes defined as $u_l = (2l - K_u)/K_u, l = 0, 1, \ldots, K_u$, and similarly for $L_j^{K_v}(v)$ and $L_k^{K_w}(w)$. Equation (1) defines a mapping from a cubical parent domain to the generalized hexahedron, as illustrated in Fig. 2. The electric field in the element, $\mathbf{E}(u, v, w)$, is approximated by means of curl-conforming hierarchical polynomial vector basis functions given in [20]; let us denote the functions by $\mathbf{f}(u, v, w)$, and the respective arbitrary field-approximation orders of the polynomial by N_u, N_v, and $N_w (N_u, N_v, N_w \geq 1)$.

Continuous variations of medium parameters in the computational model can be implemented in different ways. In our technique, however, we opt to take full advantage of the already developed Lagrange interpolating scheme for defining element spatial coordinates in (1), which can be conveniently reused to govern the change of both the complex relative permittivity and permeability, ε_r and μ_r, within the element in Fig. 2, as follows:

$$\varepsilon_\mathrm{r}(u, v, w) = \sum_{i=0}^{K_u} \sum_{j=0}^{K_v} \sum_{k=0}^{K_w} \varepsilon_{\mathrm{r},ijk} L_i^{K_u}(u) L_j^{K_v}(v) L_k^{K_w}(w) \qquad -1 \leq u, v, w \leq 1 \quad (2)$$

where $\varepsilon_{\mathrm{r},ijk} = \varepsilon_\mathrm{r}(u_i, v_j, w_k)$ are the relative permittivity values at the points defined by $(K_u + 1)(K_v + 1)(K_w + 1)$ position vectors of spatial interpolation nodes, $\mathbf{r}_{ijk}$, and similarly for μ_r. In the case of $K_u = K_v = K_w = 1$, for example, ε_r and μ_r, are trilinear functions throughout the element volume, governed by the given fixed values at 8 points—hexahedron vertices. For $K_u = K_v = K_w = 2$, the input are values for ε_r and μ_r at 27 interpolation nodes, and the corresponding profiles are triquadratic functions, and so on. This technique allows simple definitions of inhomogeneity profiles, as it utilizes the nodes already defined by the generalized hexahedral finite element mesh. Of course, the material profile is in general represented by many (large) elements in the FEM model. With such representation of materials, we then solve for the unknown field coefficients by substituting the field expansion $\mathbf{E}(u, v, w)$ in the Galerkin weak form of the curl-curl electric-field vector wave equation [20]

$$\int_V \mu_\mathrm{r}^{-1}(u, v, w)[\nabla \times \mathbf{f}(u, v, w)] \cdot [\nabla \times \mathbf{E}(u, v, w)] \mathrm{d}V - k_0^2 \int_V \varepsilon_\mathrm{r}(u, v, w) \mathbf{f}(u, v, w) \cdot \mathbf{E}(u, v, w) \mathrm{d}V = -\oint_S \mu_\mathrm{r}^{-1}(u, v, w) \mathbf{f}(u, v, w) \cdot \mathbf{n} \times [\nabla \times \mathbf{E}(u, v, w)] \mathrm{d}S \quad (3)$$

where $k_0 = \omega\sqrt{\varepsilon_0 \mu_0}$ is the free-space wave number, V is the volume of the element in Fig. 2, bounded by the surface S, and $\mathbf{n}$ is the outward unit normal on S. Once the field coefficients are found, all quantities of interest for the analysis are obtained in a straightforward manner.

III. Results and Discussion

Next, we validate the new technique for entire-domain FEM analysis of problems with continuously inhomogeneous materials and evaluate and discuss its accuracy and efficiency in two characteristic examples, that combined include both closed- and open-region structures, with both flat and curved surfaces. The general applicability, convergence of solutions, and limitations of 3-D higher order large finite elements have been discussed thoroughly in our previous work, [20], [23], [25], [28], including examples of nonuniform waveguides and cavities with arbitrary discontinuities, and structures (waveguide discontinuities and scatterers) with reentrant corners, sharp edges, and singular fields. Overall, higher order solutions are truly beneficial only for smooth regions, where large elements are possible. However, because the implemented basis functions are hierarchical, element orders in the model can also be low, so that the low-order modeling approach is actually included in the higher order modeling and both large and small elements can be combined together in the same model, but clearly our method is most suitable for problems where the most of the structure (homogeneous or inhomogeneous) can be tessellated using large higher order curved elements. All numerical results are obtained using an IBM ThinkPad T60p notebook computer with Intel T7200 Core2 CPU running at 2.0 GHz and with 2 GB of RAM under Microsoft Windows XP operating system. In all examples, polynomial orders of field approximations are chosen optimally—by performing p-refinement systematically, until negligible difference in the two consecutive solutions is observed.

The first example is a closed-region problem—a rectangular waveguide, of cross-sectional dimensions a and b, with a load in the form of a tightly fit continuously inhomogeneous dielectric slab, as shown in Fig. 3. The length of the slab and the lengths of air-filled waveguide portions on both sides of the slab, between the ports, are the same (c). The slab is lossy, with the real and imaginary parts of the relative permittivity ($\varepsilon_\mathrm{r} = \varepsilon_\mathrm{r}' - \mathrm{j}\varepsilon_\mathrm{r}''$) of the dielectric linearly changing from $\varepsilon_\mathrm{r}' = 1.2$ to $\varepsilon_\mathrm{r}' = 6$ and from $\varepsilon_\mathrm{r}'' = 0.2$ to $\varepsilon_\mathrm{r}'' = 2$, respectively, along the slab ($\mu_\mathrm{r} = 1$ everywhere), and this change is depicted in Fig. 3. Note that the loss-tangent in the material is rather large, ranging from $\tan\delta = 0.167$ to $\tan\delta = 0.333$. Waveguide walls, on the other side, are considered to be lossless. In the entire-domain FEM model of the structure, the complete loaded waveguide is modeled by three hexahedral elements of the first geometrical order [$K_u = K_v = K_w = 1$ in (1)] that coincide with the three waveguide sections, and the permittivity profile in Fig. 3 is incorporated in (2) for the central element. The optimal polynomial orders of the field approximation are $N_u = 4, N_v = 2$, and $N_w = 7$ in the central element, and $N_u = 4, N_v = 2$, and $N_w = 4$ in other two elements, with directions of local coordinates u, v, and w in elements corresponding, respectively, to element dimensions a, b, and c. This arrangement results in a total of as few as 205 FEM unknowns, and a total of only 3 seconds of computation time for the entire frequency range considered (36 frequency points).

To both validate the continuously inhomogeneous FEM model of the loaded waveguide and evaluate its efficiency against piecewise homogeneous approximate models, the results obtained by the presented technique are compared with the results of the FEM analysis of models with the slab replaced, respectively, by $N_l = 3, 4, 5$, and 7 equally thick homogeneous plate-like layers, approximating the continuously inhomogeneous profile, which is illustrated in Fig. 3 for the case of $N_l = 5$. Fig. 4 shows the magnitude of the computed modal S_{11} parameter of the waveguide, versus frequency, where we observe a monotonic convergence of the results using the layered-FEM technique toward the results of the continuous-FEM analysis as the number of layers

Authorized licensed use limited to: Branislav Notaros. Downloaded on September 2, 2009 at 04:23 from IEEE Xplore. Restrictions apply.

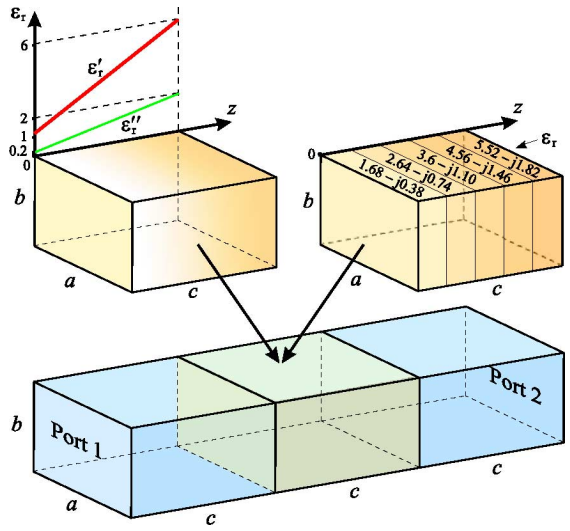

Fig. 3. Three-element higher order FEM model of a WR-15 waveguide ($a = 3.76$ mm, $b = 1.88$ mm, and $c = 2.5$ mm) with a continuously inhomogeneous lossy dielectric load (central element) whose complex permittivity varies linearly in the longitudinal direction; Five-layer model ($N_l = 5$) of the load with piecewise constant approximation of real and imaginary permittivity profiles is also shown.

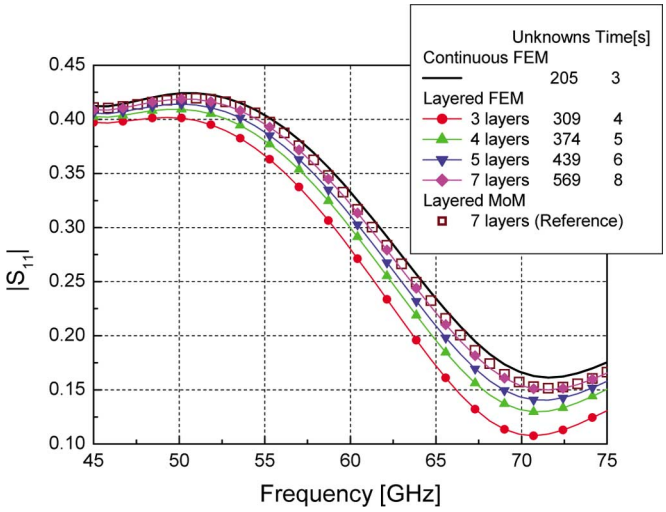

Fig. 4. Magnitude of the modal S_{11} parameter of the loaded waveguide in Fig. 3: continuous-FEM solution, layered-FEM solutions on four different piecewise homogeneous models, and reference MoM/SIE solution.

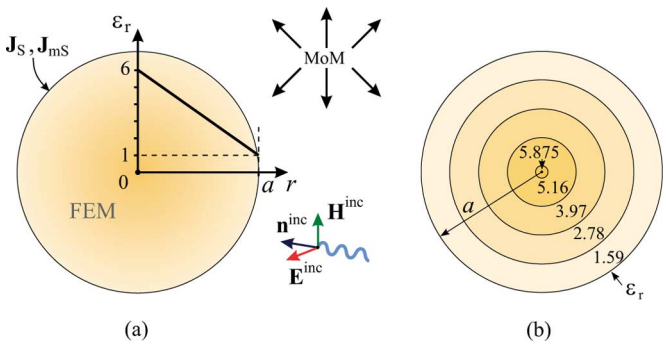

Fig. 5. FEM-MoM analysis of a continuously inhomogeneous spherical dielectric scatterer: (a) radial permittivity variation and (b) four-layer approximate model.

in the former approach is increased, with a good agreement between the 7-layer and continuous FEM solutions (theoretically, only an infinite number of layers would give the exact solution to the problem in Fig. 3). The total number of unknowns and simulation time for each of the solutions are given in the legend of Fig. 4. As an additional verification of the analysis, the 7-layer model is simulated using a higher order MoM technique based on the surface integral equation (SIE) approach (MoM/SIE technique) [27], as a reference solution, and an excellent agreement of these and the corresponding FEM results is observed. We conclude that the continuous-FEM analysis is substantially more efficient than the layered-FEM approach, which requires about 2.78 times more unknowns and 2.67 times longer computation for a lower accuracy (even more layers and unknowns are needed for a more accurate solution). Note that all results in Fig. 4 are obtained by higher order techniques, and that the advantage in the efficiency of the continuous-FEM model would be even more pronounced if compared with low-order FEM solutions on layered models. Note also that the higher order FEM simulation of the 7-layer model requires about 6 times fewer unknowns and 30 times shorter computation time than the presented higher order MoM/SIE solution. Note finally that the difference in the number of unknowns and simulation time is even larger in favor of the entire-domain FEM modeling of continuously inhomogeneous materials over piecewise homogeneous models in cases of 2-D and 3-D inhomogeneities, where the medium parameters vary in two and three dimensions, respectively.

The second example, illustrating entire-domain FEM modeling of open-region continuously inhomogeneous structures, that also possess curvature, is a lossless spherical dielectric ($\mu_r = 1$) scatterer, of radius a, and a linear radial variation of relative permittivity ($\varepsilon_r = \varepsilon_r'$) from $\varepsilon_r = 1$ at the surface to $\varepsilon_r = 6$ at the center of the sphere, as depicted in Fig. 5(a). The scatterer is situated in free space and illuminated by a uniform plane wave. To represent the permittivity variation using expansions in (2), the sphere is modeled by 7 curvilinear hexahedral FEM elements of the second geometrical order ($K_u = K_v = K_w = 2$), that is, by one small sphere-like hexahedron, $a/20$ in radius, at the center and 6 "cushion"-like hexahedra between the central sphere and the scatterer surface, onto which 6 curvilinear quadrilateral MoM patches are attached. Namely, the FEM domain is truncated at the sphere surface by means of unknown electric and magnetic surface currents, of densities $\mathbf{J}_S$ and $\mathbf{J}_{mS}$, that are evaluated by the MoM/SIE, giving rise to a hybrid higher order FEM-MoM solution [28]. The field/current approximation orders are $N_u = N_v = N_w = 5$ for all FEM "cushions" and 4 for the central FEM element and all MoM patches (in both directions), resulting in 2560 FEM and 384 MoM unknowns in the hybrid model, and a total of 976 s of simulation time for 35 frequencies.

Validation and efficiency evaluation of the continuously inhomogeneous FEM-MoM model, using large curved FEM elements with continuously changing ε_r, is carried out in comparison with solutions obtained by higher order FEM-MoM simulations of piecewise homogeneous approximate models of the structure in Fig. 5(a), where each of the six "cushions" of the continuous model are replaced, respectively, by $N_l = 2, 3, 4$, and 7 homogeneous thin "cushions" (curved plate-like layers), which approximate the continuously inhomogeneous profile, with Fig. 5(b) showing the model for $N_l = 4$. So, each spherical layer in layered models is represented by 6 FEM elements of the second geometrical order. Field-approximation orders in these elements are 2 in the radial direction and 5 in transversal directions. Shown in Fig. 6 is the monostatic radar cross section (RCS) of the sphere, normalized to λ_0^2, as a function of a/λ_0, λ_0 being the free-space wavelength. It can be observed that, with increasing N_l, the solution obtained by means of the layered-FEM-MoM technique monotonically converges to the results of the continuous-FEM-MoM analysis, as well as that the FEM-MoM solution for the 7-layer model accurately matches a

Authorized licensed use limited to: Branislav Notaros. Downloaded on September 2, 2009 at 04:23 from IEEE Xplore. Restrictions apply.

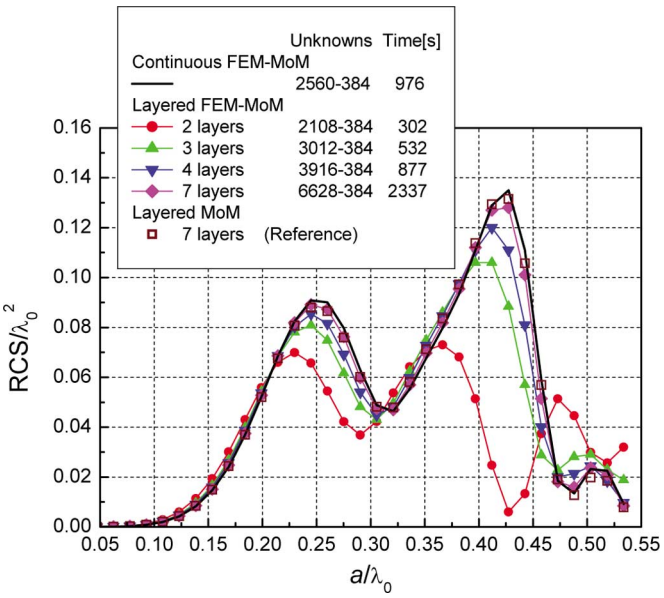

Fig. 6. Normalized monostatic radar cross section (λ_0 is the free-space wavelength) of the spherical scatterer in Fig. 5(a): results using the continuous-FEM-MoM, four different layered-FEM-MoM models, and reference MoM/SIE model.

reference pure MoM/SIE solution [27] for the same model. From the data on the numbers of unknowns (first number FEM—second number MoM) and simulation times for individual solutions given in the figure legend, we realize that the continuous material model is again substantially more efficient than the layered analysis, namely, it is about 2.39 times faster than the most accurate layered solution (for $N_l = 7$), and the reduction in the total number of unknowns is by approximately the same factor.

IV. Conclusion

This paper has presented a novel higher order entire-domain FEM technique for accurate and efficient analysis of electromagnetic structures with continuously inhomogeneous material regions, using large finite elements that allow continuous change of medium parameters throughout their volumes. The elements are Lagrange-type generalized curved parametric hexahedra of arbitrary geometrical orders with curl-conforming hierarchical polynomial vector basis functions of arbitrary field-approximation orders and Lagrange interpolating scheme for variations of medium parameters. This is the first 3-D implementation of the inherent theoretical ability of the FEM to directly treat continuously inhomogeneous materials, which allows that the material parameters can be arbitrary functions of spatial coordinates, $\varepsilon(\mathbf{r})$ and $\mu(\mathbf{r})$, in the FEM computational domain.

The examples have shown that effective higher order FEM hexahedral meshes, constructed from a very small number of large finite elements with p-refined field distributions of high approximation orders, which is one of the strongest points of the higher order modeling paradigm, can be applied even in the presence of material inhomogeneities. They have demonstrated higher efficiency, and considerable reductions in both number of unknowns and computation time, of the entire-domain FEM modeling of continuously inhomogeneous materials over piecewise homogeneous (layered) models, when higher order geometrical and field approximations are used. The advantage in the efficiency of the continuous-FEM analysis should be even more pronounced if compared with low-order FEM solutions on layered models. So, in addition to numerically demonstrating that the FEM can indeed directly treat continuously inhomogeneous materials accurately, the results have in fact indicated that large curved higher order continuous-FEM elements, being computationally efficient, also have great potential for practical applications in analysis of devices, systems, and phenomena that include material regions with pronounced inhomogeneities and complexities.

References

[1] P. P. Silvester and R. L. Ferrari, *Finite Elements for Electrical Engineers*, 3rd ed. : Cambridge Univ., 1996.
[2] J. M. Jin, *The Finite Element Method in ElectroMagn.*, 2nd ed. New York: Wiley, 2002.
[3] J. L. Volakis, A. Chatterjee, and L. C. Kempel, *Finite Element Method for ElectroMagn.*. New York: IEEE Press, 1998.
[4] A. Wexler, "Some recent developments in field calculation," *IEEE Trans. Magn.*, vol. 15, no. 6, pp. 1659–1664, Nov. 1979.
[5] C. H. Chen and C. D. Lien, "A finite element solution of the wave propagation problem for an inhomogeneous dielectric slab," *IEEE Trans. Antennas Propag.*, vol. AP-27, no. 6, pp. 877–880, Nov. 1979.
[6] V. V. Petrovic and B. D. Popovic, "Optimal FEM solutions of one-dimensional EM problems," *Inte. J. Numer. Model.: Electron. Networ., Devices and Fields*, vol. 14, pp. 49–68, 2001.
[7] M. M. Ilic and B. M. Notaros, "Trilinear hexahedral finite elements with higher-order polynomial field expansions for hybrid SIE/FE large-domain electromagnetic modeling," in *Proc. IEEE Antennas Propag. Society Int. Symp. Digest*, Boston, MA, Jul. 8–13, 2001, vol. 3, pp. 192–195.
[8] L. Vegni, F. Bilotti, and A. Toscano, "Analysis of cavity backed rectangular patch antennas with inhomogeneous chiral substrates via a FEM-BEM formulation," *IEEE Trans. Magn.*, vol. 37, no. 5, pp. 3260–3263, Sept. 2001.
[9] A. D. Greenwood and J. M. Jin, "Finite-element analysis of complex axisymmetric radiating structures," *IEEE Trans. Antennas Propag.*, vol. 47, no. 8, pp. 1260–1266, Aug. 1999.
[10] K. Davies, *Ionospheric Radio Propagation*. New York: Dover Publications, 1966.
[11] A. T. Villeneuve, "Propagation of electromagnetic waves through inhomogeneous slabs," *IEEE Trans. Antennas Propag.*, vol. AP-13, no. 6, pp. 926–933, Nov. 1965.
[12] H. Kumagami, M. Koshiba, and M. Suzuki, "Finite element analysis of planar anisotropic inhomogeneous optical waveguides," *Electron. Commun. Jpn.*, vol. 68, no. 5, pt. 2, pp. 52–60, 1985.
[13] K. Okamoto and T. Okoshi, "Vectorial wave analysis of inhomogeneous optical fibers using finite element method," *IEEE Trans. Microw. Theory Tech.*, vol. MTT-26, no. 2, pp. 109–114, Feb. 1978.
[14] I. T. Rekanos and T. D. Tsiboukis, "A combined finite element—Nonlinear conjugate gradient spatial method for the reconstruction of unknown scatterer profiles," *IEEE Trans. Magn.*, vol. 34, no. 5, pp. 2829–2832, Sept. 1998.
[15] W. C. Chen and J. M. Jin, "Perfectly matched layers in the discretized space: An analysis and optimization," *ElectroMagn.*, vol. 16, pp. 325–340, 1996.
[16] E. Michielssen, W. C. Chew, and D. S. Weile, "Genetic algorithm optimized perfectly matched layers for finite difference frequency domain applications," in *1996 IEEE Antennas Propag. Society International Symp. Digest*, July 1996, vol. 3, pp. 2106–2109.
[17] R. D. Graglia, D. R. Wilton, and A. F. Peterson, "Higher order interpolatory vector bases for computational electromagnetics," *IEEE Trans. Antennas Propag.*, vol. 45, no. 3, pp. 329–342, Mar. 1997.
[18] J. P. Webb, "Hierarchical vector basis functions of arbitrary order for triangular and tetrahedral finite elements," *IEEE Trans. Antennas Propag.*, vol. 47, no. 8, pp. 1244–1253, Aug. 1999.
[19] J. M. Jin, K. C. Donepudi, J. Liu, G. Kang, J. M. Song, and W. C. Chew, "High-order methods in computational electromagnetics," in *Fast and Efficient Algorithms in Computational ElectroMagn.*, W. C. Chew, Ed. Norwood, MA: Artech House, 2001.
[20] M. M. Ilić and B. M. Notaroš, "Higher order hierarchical curved hexahedral vector finite elements for electromagnetic modeling," *IEEE Trans. Microw. Theory Tech.*, vol. 51, no. 3, pp. 1026–1033, Mar. 2003.
[21] S. C. Lee, J. F. Lee, and R. Lee, "Hierarchical vector finite elements for analyzing waveguiding structures," *IEEE Trans. Microw. Theory Tech.*, vol. 51, no. 8, pp. 1897–1905, Aug. 2003.
[22] J. M. Jin, J. Liu, Z. Lou, and C. S. T. Liang, "A fully high-order finite-element simulation of scattering by deep cavities," *IEEE Trans. Antennas Propag.*, vol. 51, pp. 2420–2429, Sept. 2003.

Authorized licensed use limited to: Branislav Notaros. Downloaded on September 2, 2009 at 04:23 from IEEE Xplore. Restrictions apply.

[23] M. M. Ilić, A. Ž. Ilić, and B. M. Notaroš, "Higher order large-domain FEM modeling of 3-D multiport waveguide structures with arbitrary discontinuities," *IEEE Trans. Microw. Theory Tech.*, vol. 52, no. 6, pp. 1608–1614, Jun. 2004.
[24] R. D. Graglia and G. Lombardi, "Singular higher order complete vector bases for finite methods," *IEEE Trans. Antennas Propag.*, vol. 52, pp. 1672–1685, Jul. 2004.
[25] M. M. Ilić and B. M. Notaroš, "Higher order large-domain hierarchical FEM technique for electromagnetic modeling using Legendre basis functions on generalized hexahedra," *Electromagn.*, vol. 26, pp. 517–529, Oct. 2006.
[26] B. M. Notaroš, "Higher order frequency-domain computational electromagnetics," *IEEE Trans. Antennas Propag. Special Issue on Large and Multiscale Comput. Electromagn.,* , vol. 56, no. 8, pp. 2251–2276, Aug. 2008.
[27] M. Djordjević and B. M. Notaroš, "Double higher order method of moments for surface integral equation modeling of metallic and dielectric antennas and scatterers," *IEEE Trans. Antennas Propag.*, vol. 52, no. 8, pp. 2118–2129, Aug. 2004.
[28] M. M. Ilić, M. Djordjević, A. Ž. Ilić, and B. M. Notaroš, "Higher order hybrid FEM-MoM technique for analysis of antennas and scatterers," *IEEE Trans. Antennas Propag.*, to be published.

Extended Analysis of Retrodirective Cross-Eye Jamming

W. P. du Plessis, J. W. Odendaal, and J. Joubert

***Abstract*—An extended and rigorous analysis of retrodirective cross-eye jamming in a radar system scenario is presented. This analysis removes the approximations that limit the validity of other analyses of cross-eye jamming. These results imply that under certain conditions, a monopulse radar system can be more easily deceived than suggested by conventional cross-eye analyses. Furthermore, the cross-eye jammer antenna patterns do not affect the induced monopulse error.**

***Index Terms*—Electronic warfare, radar countermeasures, radar tracking.**

I. Introduction

Cross-eye jamming is an electronic warfare (EW) technique that induces an angular deception in a radar system by recreating the worst-case glint angular error [1]–[6]. The target angular error is created by transmitting out of phase signals from two or more onboard antennas, thereby deceiving the radar into believing that the target is spatially removed from its true position.

In analyzing the performance of cross-eye jamming on a radar system, the effect of cross-eye jamming is generally considered as a distortion of the phase front incident on the antenna(s) of the radar system [2]–[5] or a change in the direction of the incident Poynting vector [7]. In [8], Kajenski has shown that the phase-front and Poynting vector approaches to analyzing cross-eye jamming are equivalent. Cross-eye jamming has also been analyzed using first-order Taylor approximations to either the sum- and difference-channel antenna patterns [9], [10] or the lobes of an amplitude-comparison tracking radar system [11]. Recently, a graphical vector representation of the fields incident on a radar antenna due to cross-eye jamming was used to analyze cross-eye jamming performance [6], [12].

Manuscript received October 10, 2008; revised February 13, 2009. First published July 10, 2009; current version published September 02, 2009.

W. P. du Plessis is with the University of Pretoria, Pretoria 0002, South Africa and also with the Council for Scientific and Industrial Research (CSIR) - Defence, Peace, Safety and Security (DPSS), Pretoria Gauteng 0001, South Africa (e-mail: wduplessis@csir.co.za).

J. W. Odendaal and J. Joubert are with the Centre for Electromagnetism, University of Pretoria, Pretoria 0002, South Africa .

Digital Object Identifier 10.1109/TAP.2009.2027353

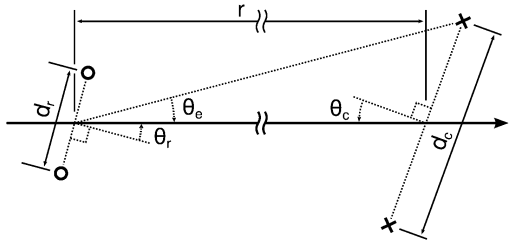

Fig. 1. The geometry used for the cross-eye jammer derivation.

These analyses assume (either directly or indirectly through the way the antenna patterns are determined) that amplitude variations over the radar antenna aperture are negligible. Another significant limitation of conventional cross-eye analyses is that they ignore the retrodirective implementation of most cross-eye systems [2], [3], [5], [6]. While retrodirective (Van Atta) arrays have been extensively considered in the literature (e.g., [13]–[19]), the work has concentrated on the issues like mutual coupling and mismatches in the array itself rather than its effects on a radar.

This communication presents the summarized results of an extended and rigorous analysis of cross-eye jamming in a monopulse radar system scenario that has recently been performed [20]. The extended analysis takes into consideration the physical separation between the antennas of a monopulse radar system and derives an expression for the induced angular error due to the cross-eye jammer. Induced angular error results that demonstrate the differences between the conventional and extended cross-eye jamming analyses are presented.

Section II outlines the derivation of the extended analysis. Section III presents a comparison between induced angular errors obtained with the classical and extended analyses, and also considers some of the more significant implications of the extended analysis. Finally, Section IV provides a brief conclusion.

II. Theory

The purpose of cross-eye jamming is to produce an angular error in a radar system, thus causing the radar to believe that the target is spatially removed from its true position. Consider the cross-eye jamming scenario shown in Fig. 1. Assume the phase-comparison monopulse radar consists of two identical antennas separated by a distance of d_r (denoted by the circles in Fig. 1). The cross-eye elements have a linear separation of d_c at a range of r giving an angular separation of $2\theta_e$ from the radar's perspective (denoted by the crosses in Fig. 1). The directions to the top and bottom cross-eye antennas are thus $\theta_r \pm \theta_e$ respectively.

While amplitude-comparison monopulse systems are not explicitly considered in this correspondence, Sherman [10] shows that amplitude- and phase-comparison monopulse systems are equivalent.

The underlying principle of cross-eye jamming is that the radar is not able to resolve the individual jammer antennas and therefore responds to their combined effect. This implies that the cross-eye jammer system is in the far field of the radar antenna ($r \gg d_r$). However, it is assumed that although the radar is in the far field of the individual jammer antenna elements, it is not in the far field of the complete cross-eye jammer system [6], [12].

0018-926X/$26.00 © 2009 IEEE

Authorized licensed use limited to: Branislav Notaros. Downloaded on September 2, 2009 at 04:23 from IEEE Xplore. Restrictions apply.